Analysis of Focusing of Pulse Modulated Microwave Signals Inside a Tissue Medium

Konstantina S. Nikita and Nikolaos K. Uzunoglu

Abstract—**The possibility to achieve focusing in a three-layer cylindrical biological tissue model, by using a large number of concentrically placed waveguide applicators and pulsed signals (~1 ns pulse width) with a high frequency (9.5 GHz) carrier is examined rigorously. The medium response to time harmonic excitation of the array is predicted, by solving the associated boundary value problem. To this end, the fields inside the tissue layers are expressed as integrals of vector cylindrical waves, satisfying the corresponding wave equations, while the fields inside the waveguides are expanded in terms of the guided and evanescent normal modes. By imposing the appropriate boundary conditions, a system of coupled integral equations is derived on the waveguide apertures, which is solved by expressing the unknown electric fields in terms of the waveguide modes and by applying a Galerkin procedure. Then, the medium response to pulse modulated excitation of the array elements is considered and the time dependence of the electromagnetic fields produced at any point within tissue is obtained in the form of an inverse Fourier integral. Numerical results are computed and presented at several points in a three-layer geometry, 20 cm in diameter, irradiated by a 30-element waveguide array and the use of time coincidence and constructive phase interference principles is examined, in order to achieve focusing at a specific point of interest within tissue.**

I. Introduction

A HIGHLY interesting topic in using microwave signals in biomedical applications is to develop techniques and systems achieving "focusing" inside tissues. Until now, only continuous wave concepts were applied to design and develop hyperthermia systems for the treatment of malignant tumors. Phased array principles [1]–[3] and optimization techniques [4]–[6] have been applied by several researchers for determining the optimal amplitude and phase excitation of the array elements in order to focus the electromagnetic field at a specific target of interest, but always with limited success, mainly because of the excessive loss suffered by each wave radiated from each individual source. Mainly the low microwave spectrum (100–1000 MHz) has been employed in this context.

In this paper, an alternative short technique to achieve focusing of pulsed signals (~1 ns pulse width) with a high frequency (9.5 GHz) carrier is examined rigorously. The possibility of employing large number of applicators compared to low frequency systems and the significantly different behavior of pulsed signals has motivated the initiation of this study. This is a problem of considerable practical importance due to the recent advances in electromagnetic source technology, which permit the generation of high-peak-power, electromagnetic pulse signals with rapid rise times and short pulse durations [7]. The current use of stereotactic external beam radiotherapy [8] and [9], which is a sophisticated technique involving high precision delivery of localized irradiation to small intracranial lesions, by using a large number of fixed or moving fields, provided the rationale for investigating in detail the possibility of achieving high energy deposition in a specific target within the human body, by focusing the pulse modulated microwave radiation of a concentric waveguide array. To this end, constructive phase interference and time coincidence of the pulse modulated microwave signals principles are applied. Therefore, it is a matter of considerable medical interest to analyze in detail the interaction of pulse modulated microwave signals of short pulse duration with biological media.

Most of the previous works analyzing the propagation of electromagnetic pulses in dispersive media have been based on the treatment of individual pulses as members of a pulse train, so that the problem is amenable to a Fourier-series analysis. In [10] and [11], a Fourier series based methodology is presented and utilized to study the dynamics of short trapezoidally modulated microwave signals inside homogeneous, dispersive biological media, from the point of view of possible hazardous health effects. The Fourier series methodology cannot provide a rigorous solution for the case of a single, compact incident pulse. The case of a single pulse has been treated by the use of asymptotic analysis [12], transform techniques [13], time-domain integral equation solvers [14], and the finite-difference time-domain algorithm [15] and [16]. In all these works the interest was mainly focused on the propagation of a single pulse modulated electromagnetic wave in dispersive dielectric media and on the study of the associated precursor fields.

In this paper, the transmission of pulse modulated microwave signals radiated from a concentric waveguide array in a three-layer cylindrical lossy model is analyzed theoretically. The complex transfer function over the frequency-space domain of interest is computed, by using an integral equation technique in order to solve the associated boundary value problem and then, the dynamic field evolution over the entire space-time domain is obtained by numerical inversion of the associated Fourier integral representation. It is important to emphasize that a detailed three-dimensional (3-D) electromagnetic model is employed, which takes into account the modification of the field on each waveguide aperture resulted from the other radiating elements of the array as well as from the presence of the lossy, layered, dielectric body standing at the near field region [17].

Manuscript received November 13, 1995; revised April 14, 1996.

The authors are with the Institute of Communication and Computer Systems, Department of Electrical and Computer Engineering, National Technical University of Athens, Athens 10682, Greece.

Publisher Item Identifier S 0018-9480(96)07025-1.

The paper is organized in the following manner. The formulation and the analysis for the prediction of the exact field evolution over the entire space–time domain of interest is presented in Section II. In Section III, the necessary checks for the validation of the numerical results are presented, followed by a set of numerical results for a specific tissue—array geometry in Section IV.

II. Mathematical Formulation and Analysis

The objective of the present work is to study the response within a layered lossy biological medium to pulse modulated microwave signals radiated by a concentric array of waveguide applicators. The system examined in this paper consists of an arbitrary number (N) of identical rectangular waveguide applicators. The geometry of the radiating system looking into a three-layer cylindrical lossy model of circular cross section is shown in Fig. 1. The three layers can be used to simulate different biological media, such as skin, bone, and brain tissue. Alternatively, the two internal layers may be used to simulate biological media (e.g., brain and bone tissues) with the external layer simulating a lossless dielectric medium, which is commonly used to prevent excessive heating of the tissue surface. The electromagnetic properties of the layers are denoted with the corresponding relative complex permittivities ε_1, ε_2, and ε_3. The free-space wavenumber is $k_0 = \omega\sqrt{\varepsilon_0\mu_0}$, where ε_0 and μ_0 are the free-space permittivity and permeability, respectively, and the whole space is assumed to be nonmagnetic with $\mu_1 = \mu_2 = \mu_3 = \mu_0$. The applicators are filled with a dielectric material of relative permittivity ε_w and relative permeability μ_w and have an aperture size of $a \times b$ ($b < a$). It is assumed that apertures are not completely planar and are placed at the periphery of the lossy model with the large dimension at the transverse direction circulating around the cylindrical surface and the small dimension parallel to the axis of the cylindrical model. Thus the entire aperture of each applicator is assumed to be in direct contact with the tissue surface. Radiating apertures are separated by perfectly conducting flanges. By considering a global cylindrical polar coordinate system ρ, φ, z, the position vector of the lth applicator's aperture center is expressed $\underline{r}_l = \rho_3\hat{\rho} + \varphi_l\hat{\varphi} + (b/2)\hat{z}$, $l = 1, 2, \cdots, N$.

An input pulse modulated harmonic signal of fixed carrier frequency ω_0 is considered to be driven to the applicators. Thus, the signal driven to the lth applicator may be represented as

$$g_l(t) = u(t)\cos(\omega_0 t + \psi_l), \quad l = 1, 2, \cdots, N \tag{1}$$

where $u(t)$ is the real-valued initial envelope function of the pulse and ψ_l is a phase term.

The spectrum of frequencies contained in the pulse modulated microwave signal is obtained from its Fourier transform

$$G_l(\omega) = \frac{1}{2\pi}\int_{-\infty}^{\infty} dt\, u(t)\cos(\omega_0 t + \psi_l)\exp(-j\omega t). \tag{2}$$

The strategy of our approach is to analyze the propagation of each frequency component individually into the structure of interest, by using Maxwell's equations, and then to obtain the dynamic field evolution over the entire space-time of interest, by computing the associated inverse Fourier integrals.

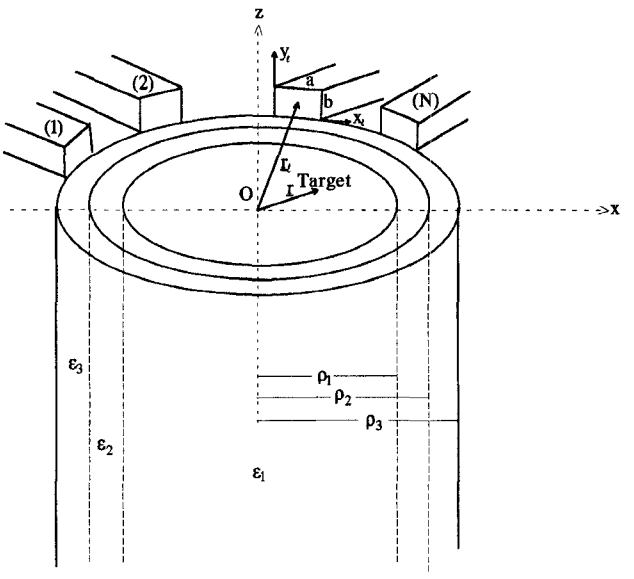

Fig. 1. Three-layer cylindrical model irradiated by a concentric array of waveguide applicators.

A. Time Harmonic Fields

The analysis begins by considering a single time harmonic component at a fixed angular frequency ω. The time dependence of the field quantities is assumed to be $\exp(+j\omega t)$ and it is suppressed throughout the analysis. In order to solve this boundary value problem, an integral equation technique is adopted.

The fields inside the tissue layers ($i = 1, 2, 3$) are written as integrals of vector cylindrical waves

$$\underline{E}_i(\underline{r}) = \int_{-\infty}^{+\infty} dk \sum_{m=-\infty}^{m=+\infty} [a_{im}\underline{M}^{(1)}_{m,k}(\underline{r}, k_i) + b_{im}\underline{N}^{(1)}_{m,k}(\underline{r}, k_i) + a'_{im}\underline{M}^{(2)}_{m,k}(\underline{r}, k_i) + b'_{im}\underline{N}^{(2)}_{m,k}(\underline{r}, k_i)] \tag{3}$$

where $k_i = k_0\sqrt{\varepsilon_i}$ and a_{im}, b_{im}, a'_{im}, b'_{im} are unknown coefficients to be determined.

In (3), $\underline{M}^{(q)}_{m,k}(\underline{r}, k_i)$, $\underline{N}^{(q)}_{m,k}(\underline{r}, k_i)$, $q = 1, 2$ [18] are the well-known vector cylindrical waves that satisfy the vector wave equation in cylindrical polar coordinates; that is

$$\nabla \times \nabla \times \begin{matrix}\underline{M}^{(q)}_{m,k}(\underline{r}, k_i) \\ \underline{N}^{(q)}_{m,k}(\underline{r}, k_i)\end{matrix} - k_i^2 \begin{matrix}\underline{M}^{(q)}_{m,k}(\underline{r}, k_i) \\ \underline{N}^{(q)}_{m,k}(\underline{r}, k_i)\end{matrix} = 0. \tag{4}$$

The fields inside each waveguide are described as the superposition of an incident TE_{10} mode and an infinite number of all the reflected TE and TM modes. Following the notation of [18], the transverse electric field inside the lth waveguide applicator ($l = 1, 2, \cdots, N$) can be written, with respect to the local Cartesian coordinates system x_l, y_l, z_l attached to

the aperture's corner (see Fig. 1), as follows:

$$\underline{E}^{w}_{l,t}(x_l, y_l, z_l) = p_l e^{j\psi_l} \underline{e}^{\mathrm{TE}}_{1,t}(x_l, y_l) \frac{j\omega\mu_0\mu_w}{u_1} e^{-j\gamma_1 z_l} + \sum_{n=1}^{\infty} \left[A'_{l,n} \underline{e}^{\mathrm{TE}}_{n,t}(x_l, y_l) \frac{j\omega\mu_0\mu_w}{u_n} e^{j\gamma_n z_l} + B'_{l,n} \underline{e}^{\mathrm{TM}}_{n,t}(x_l, y_l) \left(-\frac{j\lambda_n}{v_n}\right) e^{j\lambda_n z_l} \right] \quad (5)$$

where the subscript t is used to denote the transverse field components, $p_l e^{j\psi_l}$ is the complex amplitude of the excited TE_{10} mode in the lth waveguide, $A'_{l,n}$ and $B'_{l,n}$ are the complex amplitudes of the reflected transverse electric fields of the nth TE and nth TM modes, respectively, in the lth waveguide and γ_n, λ_n are the corresponding propagation constants, given by the following equations:

$$\gamma_n = (k_0^2\varepsilon_w - u_n^2)^{1/2}$$
$$\lambda_n = (k_0^2\varepsilon_w - v_n^2)^{1/2}. \quad (6)$$

The transverse $\underline{e}^{\mathrm{TE}}_{n,t}$ and $\underline{e}^{\mathrm{TM}}_{n,t}$ modal fields are [18]

$$\underline{e}^{\mathrm{TE}}_{n,t}(x_l, y_l) = \frac{\hat{z}_l \times \nabla_{l,t}\xi_n}{u_n}$$
$$\underline{e}^{\mathrm{TM}}_{n,t}(x_l, y_l) = \frac{\nabla_{l,t}\phi_n}{v_n} \quad (7)$$

where $\nabla_{l,t} = (\partial/\partial x_l \hat{x}_l + \partial/\partial y_l \hat{y}_l)$ and the scalar functions ξ_n and ϕ_n satisfy the wave equations

$$(\nabla^2 + u_n^2)\xi_n = 0$$
$$(\nabla^2 + v_n^2)\phi_n = 0 \quad (8)$$

and the boundary conditions

$$\frac{\partial \xi_n}{\partial n_l} = 0$$
$$\phi_n = 0 \quad (9)$$

on the walls of the waveguide, with $\partial/\partial n_l$ being the normal derivative.

By satisfying the continuity of the tangential electric and magnetic field components on the $\rho = \rho_1$ and $\rho = \rho_2$ interfaces and on the $\rho = \rho_3$ contact surface between cylindrical lossy model and radiating apertures, the following system of N coupled integral equations is obtained in terms of an unknown transverse electric field $\underline{E}_a$ on the waveguide apertures

$$\sum_{q=1}^{N} \iint_{\Gamma_q} dx'\, dy' \overline{\underline{K}}_{lq}(x, y/x', y') \underline{E}_a(x', y') = 2p_l e^{j\psi_l} \underline{h}^{\mathrm{TE}}_{1,t}\left(\frac{j\gamma_1}{u_1}\right) \quad l = 1, 2, \cdots, N/q = 1, 2, \cdots, N \quad (10)$$

where $\underline{h}^{\mathrm{TE}}_{1,t}$ is the incident TE_{10} mode transverse magnetic field on the aperture of the lth waveguide, and the kernel matrices $\overline{\underline{K}}_{lq}(x, y/x', y')$, $q = 1, \cdots, N/l = 1, \cdots, N$ indicate the effect of coupling from the qth aperture $(x', y') \in \Gamma_q$ to the lth aperture $(x, y) \in \Gamma_l$ and are given in the Appendix. In order to determine the electric field on the waveguide apertures, the system of integral equations (10) is solved. To this end a Galerkin's technique was adopted by expanding the unknown transverse electric field on each aperture $\underline{E}_{q,a}$ into waveguide normal modes. Therefore, with respect to the qth $(q = 1, 2, \cdots, N)$ aperture's corner attached local Cartesian coordinate system, the electric field on the same aperture is expressed in the following form:

$$\underline{E}_{q,a} = \sum_{n=1}^{\infty} (g_{q,n} \underline{e}^{\mathrm{TE}}_{n,t} + f_{q,n} \underline{e}^{\mathrm{TM}}_{n,t}) \quad q = 1, 2, \cdots, N. \quad (11)$$

By substituting (11) into the system of coupled integral equations (10), and making use of the waveguide modes orthogonality [18], the system of integral equations (10) is converted into an infinite system of linear equations. Assuming the $g_{q,n}$ and $f_{q,n}$ expansion coefficients are determined approximately, the aperture fields can be determined approximately by using (11) and then the coefficients a_{im}, b_{im}, a'_{im}, b'_{im} $(i = 1, 2, 3)$ of (3) are determined easily. Substituting the values of these coefficients into (3), the electric field at any point inside tissue can be easily computed.

B. Gaussian Pulse Modulation

The signals of interest in this study are modulated by a Gaussian envelope function. Thus the initial field envelope of the lth applicator is written as

$$u_l(t) = \exp\left[\frac{-(t - t_l)^2}{2\tau^2}\right], \quad l = 1, 2, \cdots, N \quad (12)$$

that is centered around the time $t_l > 0$ with a full width at e^{-1} maximum given by $2\sqrt{2}\tau$. The frequency spectrum of this initial pulse envelope is then [19]

$$U(\omega) = \sqrt{2\pi}\,\tau \exp\left(-\frac{\tau^2\omega^2}{2}\right) \exp(j\omega t_l). \quad (13)$$

The Gaussian-modulated microwave signal at a fixed angular frequency ω_0 driven to the lth applicator is given by the following equation:

$$g_l(t) = \exp\left[\frac{-(t - t_l)^2}{2\tau^2}\right] \cos(\omega_0 t + \psi_l) \quad (14)$$

and the spectrum of frequencies contained in this signal is obtained from its Fourier transform [19]. This is

$$G_l(\omega) = \frac{1}{2\pi} \int_{-\infty}^{\infty} dt \exp\left[\frac{-(t - t_l)^2}{2\tau^2}\right] \cdot \cos(\omega_0 t + \psi_l) \exp(-j\omega t)$$
$$G_l(\omega) = \frac{1}{4\pi} e^{j\psi_l} e^{-j(\omega-\omega_0)t_l} U(\omega - \omega_0) + \frac{1}{4\pi} e^{-j\psi_l} e^{-j(\omega+\omega_0)t_l} U(\omega + \omega_0) \quad (15)$$

where the modulation property and the time shifting property of the Fourier transform [19] have been used.

The instantaneous distribution of the incident field on the aperture of the lth applicator is

$$\underline{e}_l(x_l, y_l, z_l = 0; t) = p_l\, g_l(t) \underline{e}^{\mathrm{TE}}_{1,t}(x_l, y_l) \quad (16)$$

where p_l is the real amplitude of the incident TE_{10} mode driven to the lth applicator and $\underline{e}_{1,t}^{TE}(x_l, y_l)$ is the TE_{10} field distribution on the aperture.

The quantity of primary interest in this analysis is the complex transfer function $\underline{F}_l(\underline{r}; \omega), l = 1, 2, \cdots, N$ representing the field produced at point $\underline{r}$ inside tissue, when only the lth applicator is excited and the field on its aperture is a continuous time harmonic field $[\exp(+j\omega t)]$ of unit amplitude and zero phase [$p_l = 1$ and $\psi_l = 0$ in (10)]. In computing this field, by using the analysis presented in Section II-A, the power coupling to the remaining applicators of the configuration is taken into account.

It is important to observe that the transfer function $\underline{F}_l(\underline{r}; \omega)$, $l = 1, 2, \cdots, N$ depends on the relative position of the point of interest $\underline{r} = (\rho, \varphi, z)$ with respect to the lth applicator. Therefore, the transfer function at a point of interest for each applicator can be computed by exciting only one applicator and then computing the field at different points within tissue, corresponding to the different relative positions of the point of interest with respect to each individual applicator. This is

$$\begin{aligned}\underline{F}_l(\underline{r}; \omega) &= \underline{F}(\underline{r} - \underline{r}_l; \omega) \\ &= \underline{F}(\rho, \phi - \phi_l, z; \omega), \quad l = 1, 2, \cdots, N. \end{aligned} \tag{17}$$

The field transmitted from the applicators of the array at the point of interest, at the frequency ω, is obtained by the following summation over the N elements of the array

$$\underline{E}(\underline{r}; \omega) = \sum_{l=1}^{N} p_l \underline{F}_l(\underline{r}; \omega) G_l(\omega). \tag{18}$$

Then, the instantaneous field at the point of interest inside tissue, due to the pulse modulated excitation of the array elements, is obtained in the form of a Fourier inversion integral

$$\underline{E}(\underline{r}; t) = \sum_{l=1}^{N} p_l \int_{-\infty}^{\infty} d\omega \, \underline{F}_l(\underline{r}; \omega) G_l(\omega) \exp(j\omega t) \tag{19}$$

which, after making use of (15) and (17) and of the conjugate symmetry of Fourier transform [19], leads to the expression

$$\begin{aligned}\underline{E}(\underline{r}; t) = \frac{1}{2\pi} \mathrm{Re} \Bigg\{ & \exp(j\omega_0 t) \sum_{l=1}^{N} p_l \exp(j\psi_l) \\ & \cdot \int_{-(\Delta\omega/2)}^{\Delta\omega/2} d\omega \, \underline{F}(\rho, \phi - \phi_l, z; \omega_0 + \omega) \\ & \cdot U(\omega) \exp[j\omega(t - t_l)] \Bigg\} \end{aligned} \tag{20}$$

where the infinite upper and lower frequency limits of (19) have been replaced by $\Delta\omega/2$ and $-\Delta\omega/2$, with $\Delta\omega$ being the frequency bandwidth of the incident Gaussian pulses.

III. Validation of the Numerical Results

The method developed here has been applied to investigate the focusing ability of a 30 element–applicator concentric array at a point of interest inside a two-layer cylindrical biological tissue model, 16 cm in diameter, surrounded by a lossless dielectric layer. The two layers of the biological tissue model are used to simulate bone and brain tissues. The thicknesses of the bone and the external dielectric layers are taken to be $\rho_2 - \rho_1 = 0.5$ cm and $\rho_3 - \rho_2 = 2.0$ cm, respectively ($2\rho_3 = 20.0cm$). The complex relative permittivities of the tissue media, which are compiled from the relevant literature [20], as well as the dielectric constant of the external layer used in the calculations, are defined in Table I. The applicators have an orthogonal aperture of 2×1 cm^2 size and are placed symmetrically at the periphery of the external dielectric layer. The position vectors of their centers are $\underline{r}_l = 10\,(\mathrm{cm})\hat{\rho} + \varphi_l\hat{\varphi} + 0.5\,(\mathrm{cm})\hat{z}$, $l = 1, 2, \cdots, 30$ with $\varphi_1 = 0°$, $\varphi_2 = 12°$, $\varphi_3 = 24°, \cdots, \varphi_{30} = 348°$.

TABLE I
Electrical Parameters at 37°C at the Frequency Range 9.8–10.2 GHz

	Dielectric constant	Conductivity (S/m)
external layer	2.1	0
bone	4.0	0.42
brain	35.0	6.25

The input signal driven to each applicator is considered to be a pulse modulated microwave signal. A time-dependent Gaussian pulse of 1 ns pulse width at 10 dB was used as the amplitude modulating signal of a time harmonic microwave carrier of fixed frequency 9.5 GHz. The modulated signal had a frequency content with components in excess of 1.4 GHz, centered at 9.5 GHz.

In order to check the developed numerical code, several trials have been performed. In the first place, the computation of the transfer function, by using the analysis presented in Section II-A, has been checked. Regarding the numerical evaluation of the kernel matrix elements $\underline{K}_{lq}(x, y/x', y')$ given in the Appendix, the infinite summation with respect to the order m of Bessel's functions in the expression of fields inside the tissue layers [(3)] is computed, by truncating as high as $m \sim 40$ and the infinite integral $\int_{-\infty}^{\infty} dk$ obtained then, is computed by applying a multisegment 12 point Gaussian quadrature rule integration algorithm. The bounds of the integral are truncated as high as $k \sim 30k_0$ to attain good convergence. It is important to emphasize that the most crucial problem in developing a highly accurate algorithm for the evaluation of the kernel matrix elements, is the computation of the cylindrical functions involved to desired accuracy for arbitrary order and argument. Bessel's functions $J_m(\alpha_i\rho)$, $\alpha_i = (k_i^2 - k^2)^{1/2}$ for large k values behave as modified Bessel's functions, growing exponentially for arguments $\to\infty$. A rather efficient approach, which has been adopted, is to proceed directly with the calculation of the $[\partial J_m(\alpha_i\rho)/\partial\rho]/[J_m(\alpha_i\rho)]$ type of forms involved, by using the continued fraction rule.

The convergence and stability of the solution in the frequency domain have been examined by increasing the number of modes included in the aperture electric fields $\underline{E}_{q,a}$ [(11)]. The subset of modes (TE_{10}, TE_{12}, TE_{30}, TE_{32}, TM_{12}, and TM_{32}) appearing on applicator apertures have been considered to be sufficient to assure convergence of the solution. The continuity of the tangential fields at the $\rho = \rho_1$ and $\rho = \rho_2$ interface planes between different layers as well as on the contact surface $\rho = \rho_3$ of the external dielectric layer with the radiating apertures has been checked and verified numerically.

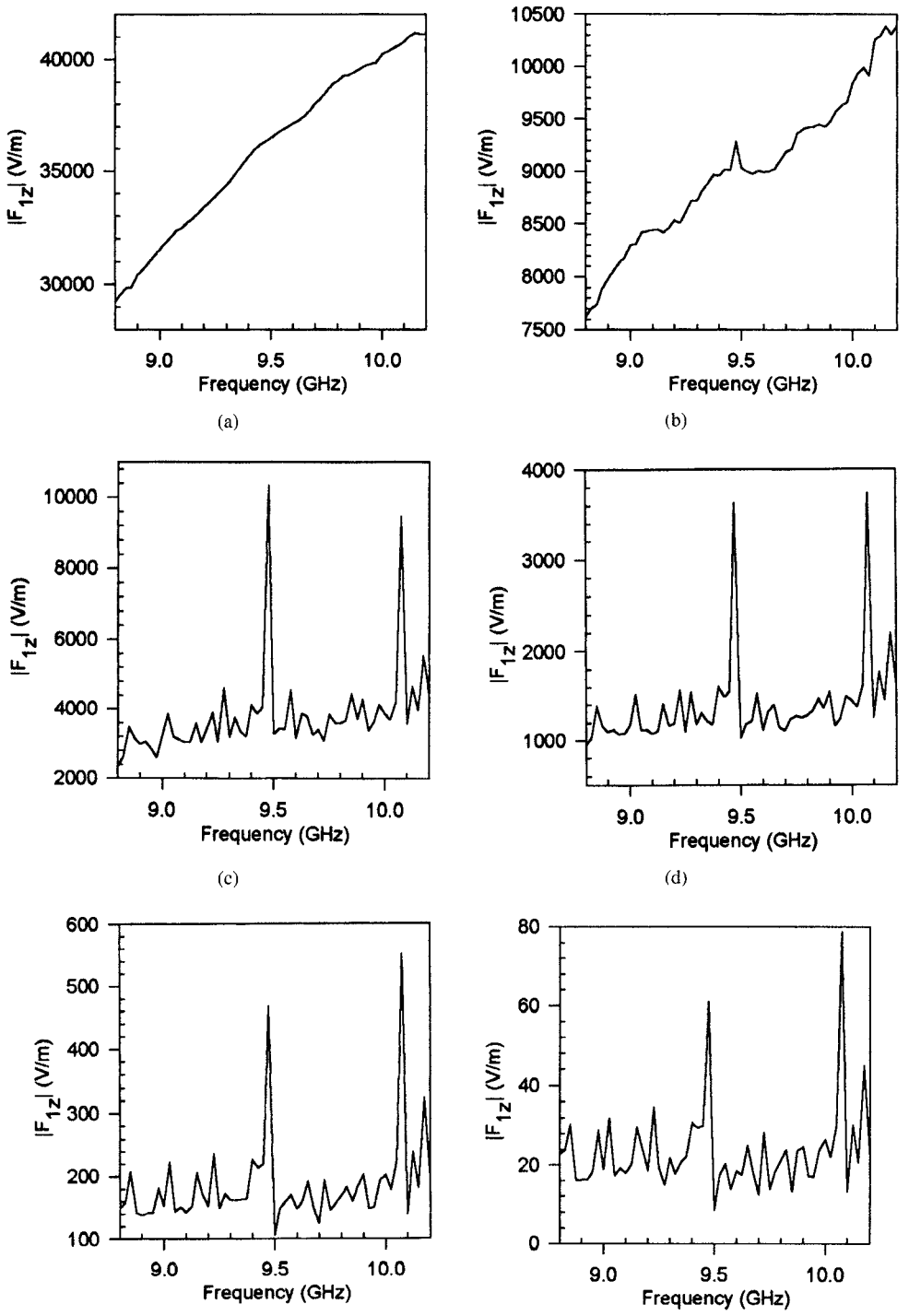

Fig. 2. A two-layer tissue model, 16 cm in diameter, simulating bone and brain tissues, surrounded by a 2-cm-thick lossless dielectric layer, is irradiated by a concentric array of 30 waveguides with an aperture size of 2×1 cm^2. The input signals driven to the individual applicators are considered to be Gaussian-modulated harmonic fields with initial pulse width 1 ns and carrier frequency 9.5 GHz. The magnitude of the main component of the transfer function at several positions on the axis of radiating aperture (1) ($|F_{1z}|$), for uniform array excitation. (a) On the surface of the dielectric layer, (b) on the interface between dielectric and bone layers, (c) on the interface between bone and brain layers, (d) at 1 cm propagation distance inside tissue, (e) at 2 cm propagation distance inside tissue, and (f) at 3 cm propagation distance inside tissue.

It is important to emphasize the fact that the developed analysis takes into account the effects on each aperture field from the other radiating elements and from the layered, dielectric cylinder standing at the near field region. The exact knowledge of the electric field at the apertures permits the evaluation of the electric field inside tissue with high precision. Note also, that although the cylindrical body is homogeneous along the z-axis, the electromagnetic field distribution varies with the z coordinate and thus, in the presented model a 3-D distribution is encountered for the electromagnetic field.

In order to compute the temporal evolution of the fields, a Simpson-rule integration algorithm has been applied to

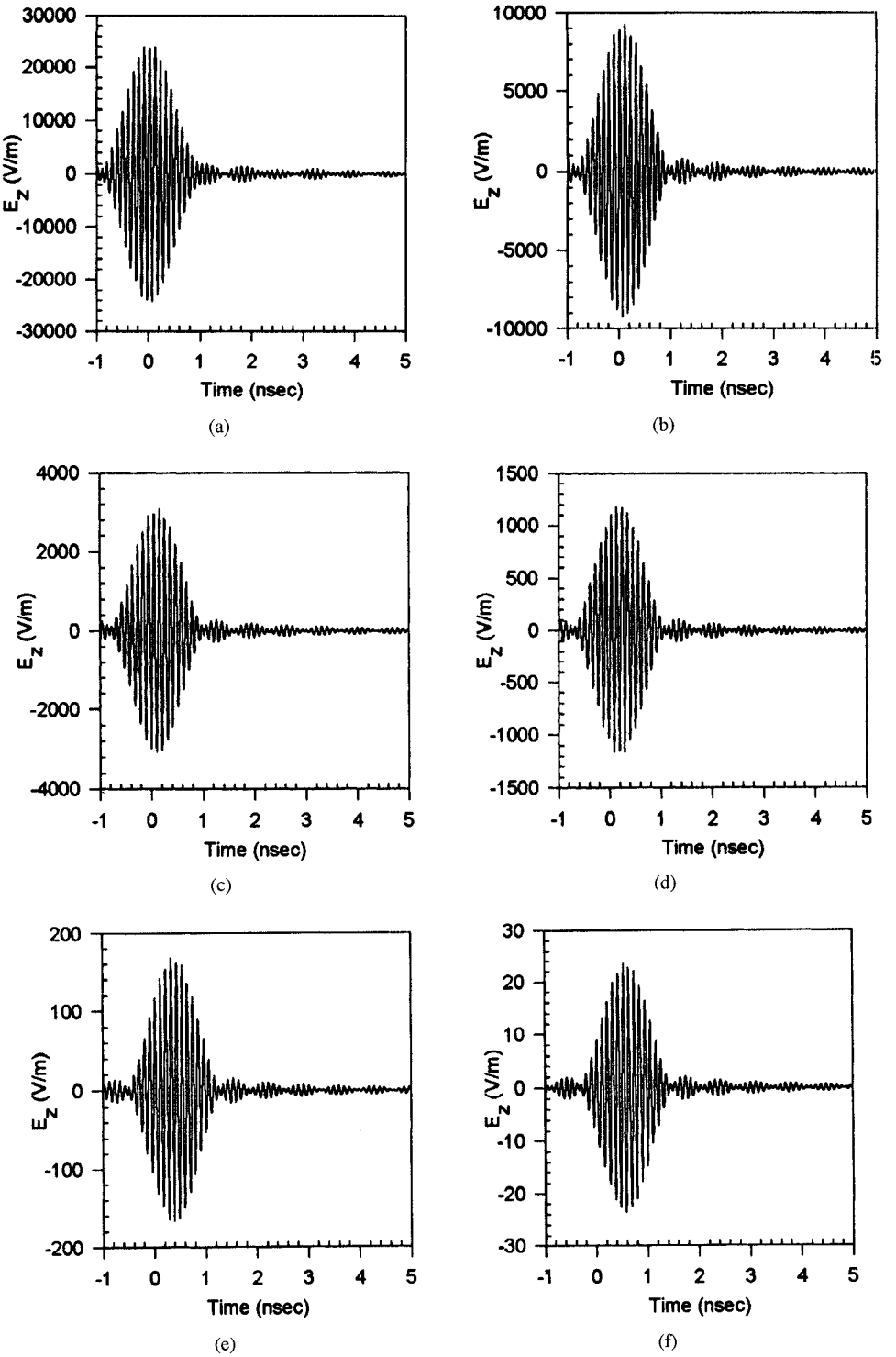

Fig. 3. Temporal evolution of the main component (E_z) of the field along the axis of aperture (1), for uniform excitation of the array. (a) On the surface of the external dielectric layer, (b) on the surface of the bone layer, (c) at the interface between bone and brain tissues, (d) at 1 cm propagation distance inside tissue, (e) at 2 cm propagation distance inside tissue, and (f) at 3 cm propagation distance inside tissue.

numerically evaluate the Fourier inversion integral of (20). Convergence checks have been performed by increasing the number of frequency intervals used in the Simpson integration algorithm. It has been observed that a frequency sampling interval of 25 MHz ensures sufficient accuracy. Moreover, by selecting a sufficiently small frequency step in computing the Fourier inversion integral, aliasing effects are minimized [19].

IV. Numerical Results and Discussion

Numerical computations have been performed for the geometry described in Section IV. First, by using the analysis presented in Section II-A, the complex transfer function $\underline{F}(\rho, \varphi - \varphi_l, z; \omega)$, $l = 1, 2, \cdots, N$ at any point inside the cylindrical model can be computed. In Fig. 2(a)–(f) the magnitude of the main (z) component of the transfer function

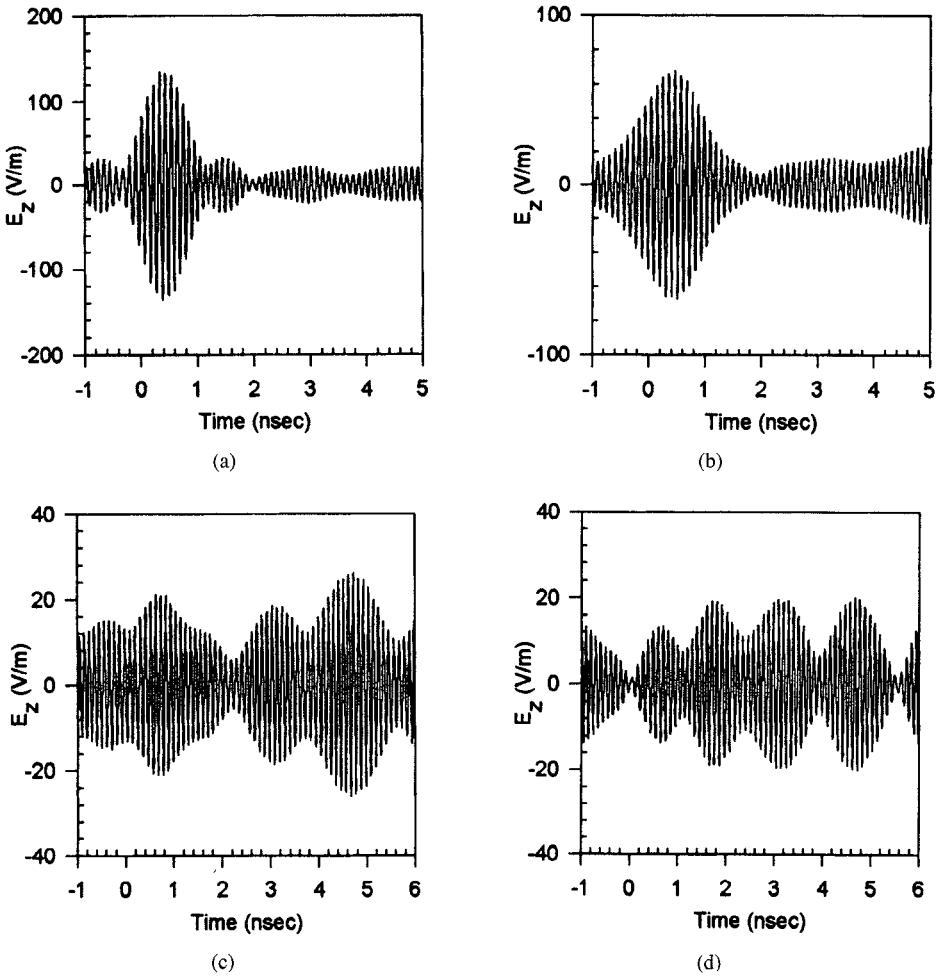

Fig. 4. Temporal evolution of the main component of the field (E_z) produced at a point of interest, located at 2 cm depth inside tissue, on the axis of applicator (1), when only one applicator of the array is excited. (a)–(d) Successive excitation of applicators (1)–(8).

is shown at different points on the axis of radiating aperture (1), inside the dielectric layer and the tissue media, over the frequency bandwidth of the used signals. On the surface of the dielectric layer, the amplitude of the transfer function increases with increasing frequency, reaching its maximum value at the high edge of the frequency spectrum, where the transmitted power from the waveguide into the dielectric becomes larger and thus the waveguide radiation more effective.

As the pulse proceeds deeper into the lossy model, the amplitudes of the individual frequency components decay in different rates with distance and selective resonance phenomena are observed at 9.5 and 10.1 GHz. At the bone-brain interface, the resonance at the carrier frequency is slightly stronger, but as the propagation distance increases, the resonance at 10.1 GHz becomes stronger than the corresponding resonance at the carrier frequency, and at 3 cm depth from the tissue surface a 2 dB difference is observed. For all the other frequencies of the incident pulses bandwidth, the attenuation is higher and the difference between them and the resonance components is of the order of 4–5 dB.

Then, the time domain waveforms at the same points along the axis of applicator (1) can be computed by using (20) and are presented in Fig. 3(a)–(f), for uniform amplitude, phase, and temporal excitation ($p_1 = \cdots = p_{30} = 1$, $\psi_1 = \cdots = \psi_{30} = 0$, and $t_1 = \cdots = t_{30} = 0$) of the array. The waveform in Fig. 3(a) was computed at a position immediately following the contact surface between aperture (1) and the external dielectric layer at the aperture center, while in Fig. 3(b)–(f) the temporal evolution of the pulse modulated fields propagating inside the tissue layers along the axis of applicator (1) is shown. A 60% decrease in the peak amplitude of the pulse is observed after the 2 cm propagation distance inside the external dielectric layer, while a 70% decrease is observed for the 0.5 cm propagation inside bone layer, a 60% decrease for the first 0.5 cm propagation inside brain tissue and a 85% decrease for the next 1 cm propagation inside brain.

In an attempt to focus the electromagnetic radiation at a point of interest, $\underline{r} = 6\hat{\rho} + 0.5\hat{z}\,(\mathrm{cm})$, within the brain tissue, located at 2 cm depth from the tissue surface on the axis of applicator (1), constructive phase interference and time coincidence of the fields originated from the 30 waveguides of the array are used. To this end, the transfer function of each individual applicator is computed and the phase of the transfer function at the carrier frequency is used to determine the appropriate phase excitation for the elements of the array in order to achieve constructive phase interference at the point of interest.

Furthermore, the temporal evolution of the main component E_z of the field originated from each individual applicator at the point of interest is examined in detail in Figs. 4(a)–(h) and

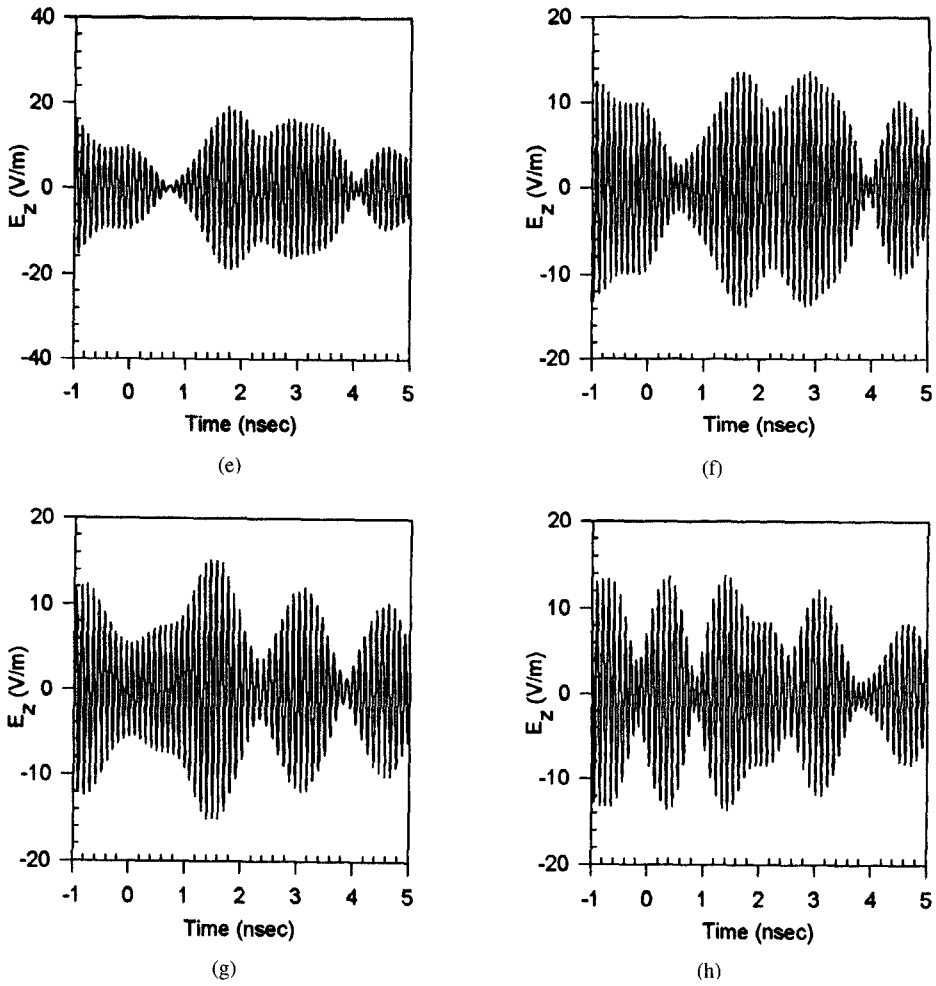

Fig. 4. *(Continued.)* Temporal evolution of the main component of the field (E_z) produced at a point of interest, located at 2 cm depth inside tissue, on the axis of applicator (1), when only one applicator of the array is excited. (e)–(h) Successive excitation of applicators (1)–(8).

5(a)–(h). Due to the x-axis symmetry and to the fact that the axes of applicators (1) and (16) coincide to the x-axis, only the fields produced from applicators (1)–(16) of the array are presented. It can be observed that the main contribution is from the most neighboring to the point of interest array elements [applicators (1) and (2)]. The field produced from more distant applicators presents secondary peaks, which are comparable in strength with the main peak of the pulse. This effect can be explained by considering the power coupling through the apertures of the array and the scattering phenomena occurring in the examined geometry.

By adjusting the phase excitation as follows:

$$\psi_1 = 14.7^\circ$$
$$\psi_2 = \psi_{30} = 109^\circ$$
$$\psi_3 = \psi_{29} = -60^\circ$$
$$\psi_4 = \psi_{28} = -143^\circ$$
$$\psi_5 = \psi_{27} = -106^\circ$$
$$\psi_6 = \psi_{26} = 88^\circ$$
$$\psi_7 = \psi_{25} = -92^\circ$$
$$\psi_8 = \psi_{24} = 60^\circ$$
$$\psi_9 = \psi_{23} = 92^\circ$$
$$\psi_{10} = \psi_{22} = -100^\circ$$
$$\psi_{11} = \psi_{21} = 89^\circ$$
$$\psi_{12} = \psi_{20} = -67^\circ$$
$$\psi_{13} = \psi_{19} = 135^\circ$$
$$\psi_{14} = \psi_{18} = -80^\circ$$
$$\psi_{15} = \psi_{17} = 88^\circ$$
$$\psi_{16} = -95^\circ$$

and introducing the following time delays in the pulse signals driven to the applicators

$$t_1 = 0.38\,\text{ns}$$
$$t_2 = t_{30} = 0.42\,\text{ns}$$
$$t_3 = t_{29} = 4.65\,\text{ns}$$
$$t_4 = t_{28} = 1.7\,\text{ns}$$
$$t_5 = t_{27} = 1.8\,\text{ns}$$
$$t_6 = t_{26} = 1.8\,\text{ns}$$
$$t_7 = t_{25} = 1.6\,\text{ns}$$
$$t_8 = t_{24} = 0.5\,\text{ns}$$
$$t_9 = t_{23} = 0.4\,\text{ns}$$
$$t_{10} = t_{22} = 2.1\,\text{ns}$$
$$t_{11} = t_{21} = 2.25\,\text{ns}$$

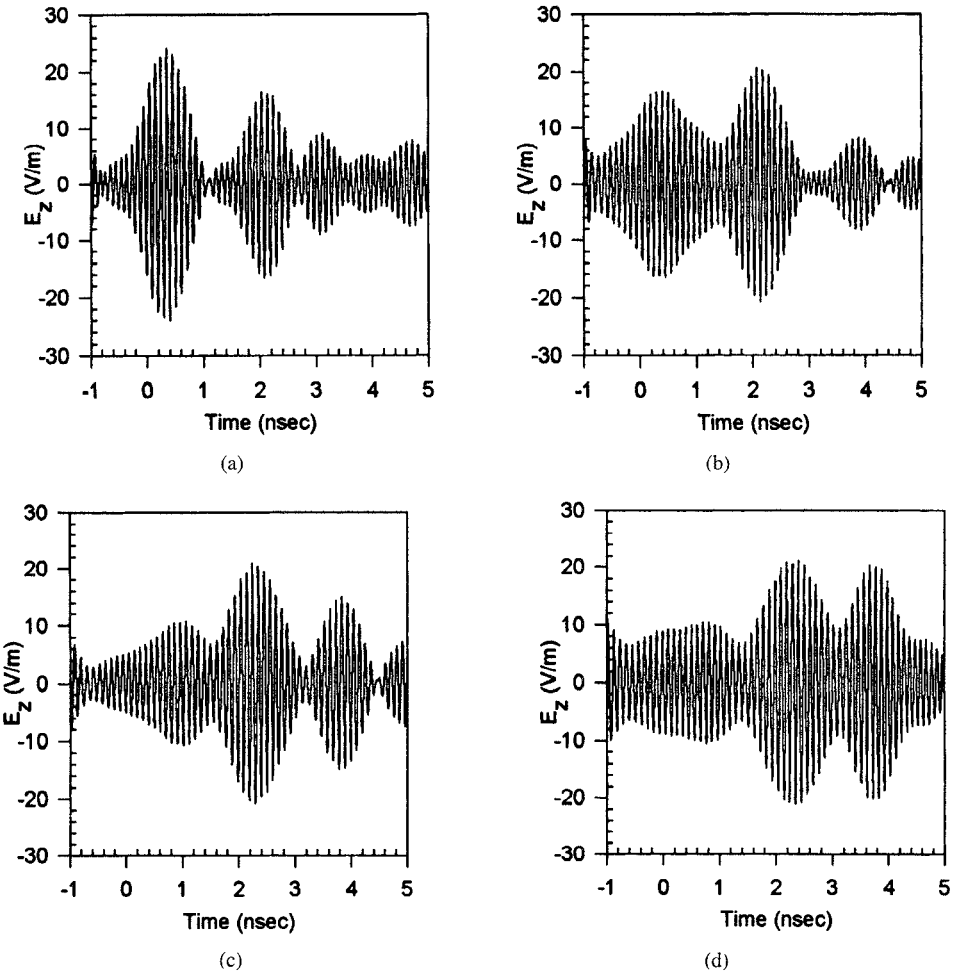

Fig. 5. Temporal evolution of the main component of the field (E_z) produced at a point of interest, located at 2 cm depth inside tissue, on the axis of applicator (1), when only one applicator of the array is excited. (a)–(d) Successive excitation of applicators (9)–(16).

$$t_{12} = t_{20} = 2.3\,\text{ns}$$
$$t_{13} = t_{19} = 3.7\,\text{ns}$$
$$t_{14} = t_{18} = 0.4\,\text{ns}$$
$$t_{15} = t_{17} = 0.4\,\text{ns}$$
$$t_{16} = 4.1\,\text{ns}$$

the time dependence of the field produced at the point of interest is shown in Fig. 6, for uniform amplitude excitation of the array elements ($p_1 = \cdots = p_{30} = 1$). By comparison of Fig. 6 with Fig. 3(e), representing the time dependence of the field at the point of interest for uniform array excitation, a 500% increase of the main peak amplitude of the pulse is achieved by adjusting the phase of the carrier frequency and the time delay of the pulse modulated signals driven to the individual applicators. Moreover, in Fig. 6 the magnitude of secondary peak amplitudes is comparable (60%) with the primary peak amplitude.

V. Conclusion

A rigorous analysis has been presented for predicting the electromagnetic field produced in a layered cylindrical lossy model by a large number of concentrically placed waveguide applicators, excited by pulse modulated microwave signals. Numerical results have been computed and presented for a bone-brain tissue model irradiated by a 30-element array, by considering input signals at a high carrier frequency (9.5 GHz) modulated by a Gaussian pulse of short pulse width (~1 ns). By adjusting the carrier phase and the time delay of the signals injected to the individual applicators, focusing at a target point within brain tissue has been achieved. These results provide an enhanced physical insight of pulse propagation inside layered lossy media and can be used in order to achieve focusing inside biological tissue media.

Appendix
Kernel Matrix Functions $\overline{\underline{K}}_{lq}(x, y/x', y')$

$$\overline{\underline{K}}_{lq}(x, y/x', y') = \int_{-\infty}^{+\infty} dk \sum_{m=-\infty}^{+\infty} e^{jm(\varphi_e - \varphi_q)} e^{jm[-(x/\rho_3)+(x'/\rho_3)]} \cdot e^{jk(y-y')} \overline{\underline{N}}(m, k) - \delta_{lq} \overline{\underline{\Omega}}(x, y/x', y') \quad l = 1, 2, \cdots, N; \quad q = 1, 2, \cdots, N \tag{A1}$$

where δ_{lq} is the Kronecker's delta

$$\overline{\underline{\Omega}}(x, y/x', y') = \sum_{n=1}^{\infty} \left\{ \left(-\frac{\gamma_n}{\omega \mu_0 \mu_w} \right) \underline{h}_{n,t}^{\text{TE}} \underline{e}_{n,t}^{\text{TE}} + \left(\frac{\omega \varepsilon_0 \varepsilon_w}{\lambda_n} \right) \underline{h}_{n,t}^{\text{TM}} \underline{e}_{n,t}^{\text{TM}} \right\} \tag{A2}$$

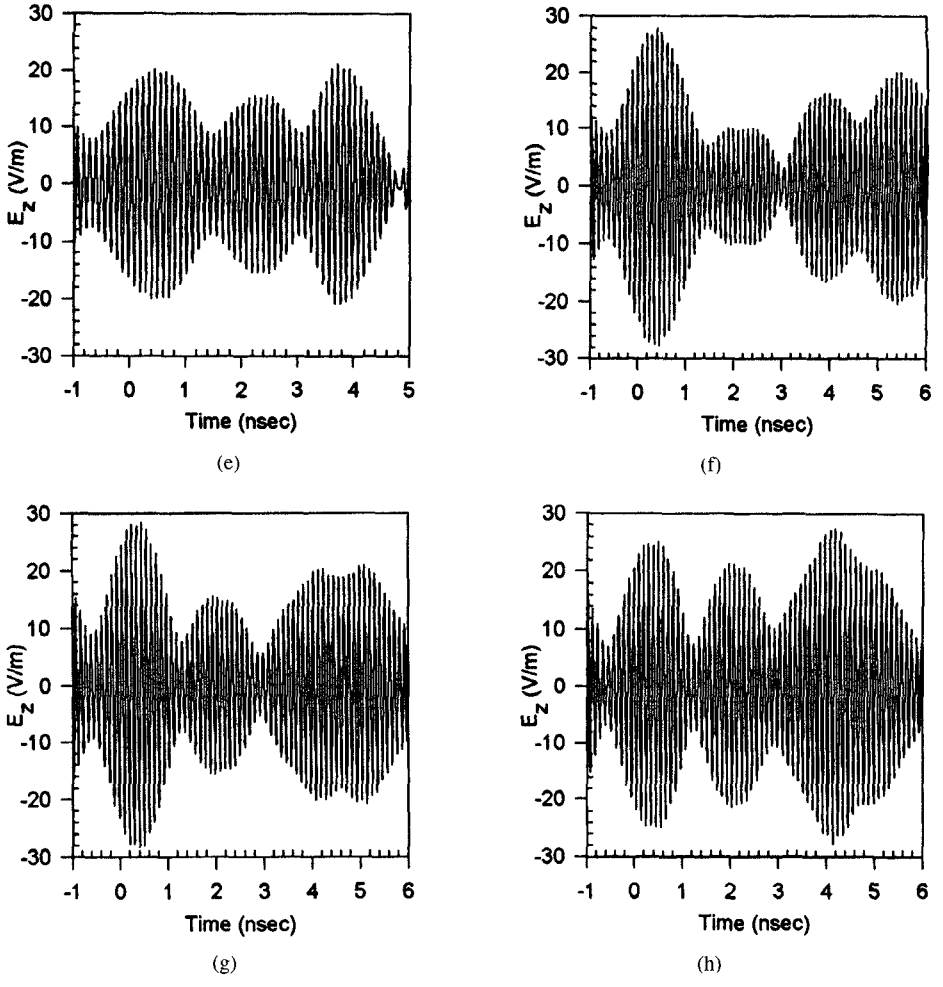

Fig. 5. *(Continued.)* Temporal evolution of the main component of the field (E_z) produced at a point of interest, located at 2 cm depth inside tissue, on the axis of applicator (1), when only one applicator of the array is excited. (e)–(h) Successive excitation of applicators (9)–(16).

$$\overline{\underline{N}}(m, k) = \frac{1}{(2\pi)^2} \frac{jk_3}{\omega\mu_0\mu_3\rho_3} \overline{\underline{L}}'(m, k; \rho_3) [\overline{\underline{L}}(m, k; \rho_3)]^{-1}. \quad \text{(A3)}$$

The matrices involved in (A3) are given by the following equations:

$$\overline{\underline{L}}'(m, k; \rho_3) = \overline{\underline{T}}_{3m}^{(1)}(k; \rho_3) + \frac{Z_m^{(2)}(\alpha_3\rho_3)}{Z_m^{(1)}(\alpha_3\rho_3)} \cdot \overline{\underline{T}}_{3m}^{(2)}(k; \rho_3) \overline{\underline{R}}_{3m} \quad \text{(A4)}$$

$$\overline{\underline{L}}(m, k; \rho) = \overline{\underline{D}}_{3m}^{(1)} + \frac{Z_m^{(2)}(\alpha_3\rho)}{Z_m^{(1)}(\alpha_3\rho)} \overline{\underline{D}}_{3m}^{(2)} \overline{\underline{R}}_{3m} \quad \text{(A5)}$$

where

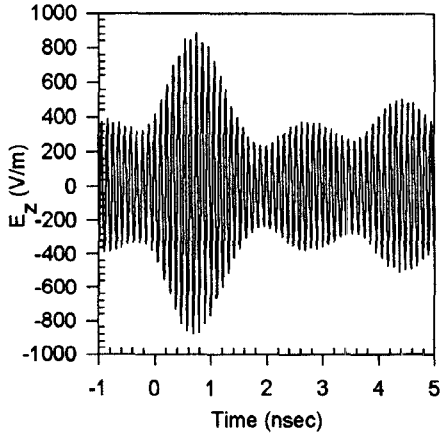

Fig. 6. Temporal evolution of the main field component (E_z) at the point of interest, when the array excitation is adjusted for focusing at this point.

$$\overline{\underline{D}}_{im}^{(q)}(k; \rho) = \begin{bmatrix} -\dfrac{\dfrac{\partial Z_m^{(q)}(\alpha_i\rho)}{\partial\rho}}{Z_m^{(q)}(\alpha_i\rho)} & -\dfrac{mk}{k_i\rho} \\ 0 & \dfrac{\alpha_i^2}{k_i} \end{bmatrix} \quad i = 3/q = 1, 2 \quad \text{(A6)}$$

$$\overline{\underline{T}}_{im}^{(q)}(k; \rho) = \begin{bmatrix} -\dfrac{mk}{k_i\rho} & -\dfrac{\dfrac{\partial Z_m^{(q)}(\alpha_i\rho)}{\partial\rho}}{Z_m^{(q)}(\alpha_i\rho)} \\ \dfrac{\alpha_i^2}{k_i} & 0 \end{bmatrix}, \quad i = 3/q = 1, 2 \quad \text{(A7)}$$

with

$$Z_m^{(1)}(\alpha_i\rho) = J_m(\alpha_i\rho)$$

and

$$Z_m^{(2)}(\alpha_i\rho) = Y_m(\alpha_i\rho), \quad \alpha_i = (k_i^2 - k^2)^{1/2} \tag{A8}$$

being Bessel's or Neuman's functions respectively, and

$$\underline{\overline{R}}_{3m} = \frac{Z_m^{(1)}(\alpha_3\rho)}{Z_m^{(2)}(\alpha_3\rho)} \left[\underline{\overline{T}}_{3m}^{(2)} - \frac{k_2}{k_3}\underline{\overline{G}}_{2m}\underline{\overline{F}}_{2m}\underline{\overline{D}}_{3m}^{(2)}\right]^{-1} \cdot \left[-\underline{\overline{T}}_{3m}^{(1)} + \frac{k_2}{k_3}\underline{\overline{G}}_{2m}\underline{\overline{F}}_{2m}\underline{\overline{D}}_{3m}^{(1)}\right] \text{ at } \rho = \rho_2. \tag{A9}$$

The matrices involved in (A9) are

$$\underline{\overline{G}}_{2m}(k;\rho) = \underline{\overline{T}}_{2m}^{(1)} + \frac{Z_m^{(2)}(\alpha_2\rho)}{Z_m^{(1)}(\alpha_2\rho)}\underline{\overline{T}}_{2m}^{(2)}\underline{\overline{R}}_{2m} \tag{A10}$$

$$\underline{\overline{F}}_{2m}(k;\rho) = \left[\underline{\overline{D}}_{2m}^{(1)} + \frac{Z_m^{(2)}(\alpha_2\rho)}{Z_m^{(1)}(\alpha_2\rho)}\underline{\overline{D}}_{2m}^{(2)}\underline{\overline{R}}_{2m}\right]^{-1} \tag{A11}$$

$$\underline{\overline{R}}_{2m} = \frac{Z_m^{(1)}(\alpha_2\rho)}{Z_m^{(2)}(\alpha_2\rho)} \cdot \left\{\underline{\overline{T}}_{2m}^{(2)} - \frac{k_1}{k_2}\underline{\overline{T}}_{1m}^{(1)}[\underline{\overline{D}}_{1m}^{(1)}]^{-1}\underline{\overline{D}}_{2m}^{(2)}\right\}^{-1} \cdot \left\{\frac{k_1}{k_2}\underline{\overline{T}}_{1m}^{(1)}[\underline{\overline{D}}_{1m}^{(1)}]^{-1}\underline{\overline{D}}_{2m}^{(1)} - \underline{\overline{T}}_{2m}^{(1)}\right\} \text{ at } \rho = \rho_1. \tag{A12}$$

The matrices $\underline{\overline{D}}_{im}^{(q)}$, $\underline{\overline{T}}_{im}^{(q)}$, $i = 1, 2$ and $q = 1, 2$, appearing in (A12), are obtained from (A6) and (A7), respectively, for $i = 1, 2$.

REFERENCES

[1] G. Arcangeli, P. P. Lombardini, G. A. Lovisolo, G. Marsiglia, and M. Piatelli, "Focusing of 915 MHz electromagnetic power on deep human tissues," *IEEE Trans. Biomed. Eng.*, vol. 31, pp. 47–52, 1984.

[2] P. F. Turner, "Mini-annular phased array for limb hyperthermia," *IEEE Trans. Microwave Theory Tech.*, vol. MTT-34, pp. 508–513, 1986.

[3] J. Chen and O. P. Ghandhi, "Numerical simulation of annular phased arrays of dipoles for hyperthermia of deep seated tumors," *IEEE Trans. Biomed. Eng.*, vol. 39, pp. 209–216, 1992.

[4] K. S. Nikita, N. G. Maratos, and N. K. Uzunoglu, "Optimal steady-state temperature distribution for a phased array hyperthermia system," *IEEE Trans. Biomed. Eng.*, vol. 40, pp. 1299–1306, 1993.

[5] J. W. Strohbehn, E. H. Curtis, K. D. Paulsen, and D. R. Lynch, "Optimization of the absorbed power distributions for an annular phased array hyperthermia system," *Int. J. Radiat. Oncol. Biol. Physics,* vol. 16, pp. 589–599, 1990.

[6] A. Boag, Y. Leviatan, and A. Boag, "Analysis and optimization of waveguide multiapplicator hyperthermia systems," *IEEE Trans. Biomed. Eng.*, vol. 40, pp. 946–952, 1993.

[7] J. Benford and J. Swengle, *High Power Microwaves.* Boston, MA: Artech, 1992.

[8] J. Graham, A. Nahum, and M. Brada, "A comparison of techniques for stereotactic radiotherapy by linear accelerator based on three-dimensional dose distribution," *Radiotherapy and Oncology,* vol. 22, pp. 29–35, 1991.

[9] S. S. Gill, D. G. T. Thomas, A. P. Warrington, and M. Brada, "Relocatable frame for stereotactic external beam radiotherapy," *Int. J. Radiat. Oncol. Biol. Physics,* vol. 20, pp. 599–603, 1991.

[10] R. Albanese, J. Penn, and R. Medina, "Short-rise-time microwave pulse propagation through dispersive biological media," *J. Opt. Soc. Am. A,* vol. 6, pp. 1441–1446, 1989.

[11] J. G. Blashank and J. Frazen, "Precursor propagation in dispersive media from short-rise-time pulses at oblique incidence," *J. Opt. Soc. Am. A,* vol. 12, pp. 1501–1512, 1995.

[12] K. E. Oughstun and J. E. K. Laurens, "Asymptotic description of electromagnetic pulse propagation in a linear causally dispersive medium," *Radio Sci.,* vol. 26, pp. 245–258, 1991.

[13] P. Wyns, D. P. Fotty, and K. E. Oughstun, "Numerical analysis of the precursor fields in linear dispersive pulse propagation," *J. Opt. Soc. Am. A,* vol. 6, pp. 1421–1429, 1989.

[14] J. Bolomey, C. Durix, and D. Lesselier, "Time domain integral equation approach for inhomogeneous and dispersive slab problems," *IEEE Trans. Antennas Propagat.,* vol. 26, pp. 658–667, 1978.

[15] R. Joseph, S. Hagness, and A. Taflove, "Direct time integration of Maxwell's equations in linear dispersive media with absorption for scattering and propagation of femtosecond electromagnetic pulses," *Opt. Lett.,* vol. 16, pp. 1412–1414, 1991.

[16] R. J. Luebbers and F. Hunsberger, "FD-TD for n-th order dispersive media," *IEEE Trans. Antennas Propagat.,* vol. 40, pp. 1297–1301, 1992.

[17] K. S. Nikita and N. K. Uzunoglu, "Coupling phenomena in concentric multiapplicator phased array hyperthermia systems," *IEEE Trans. Microwave Theory Tech.,* vol. 44, no. 1, pp. 65–74, Jan. 1996.

[18] D. S. Jones, Theory of Electromagnetism. Oxford: Pergamon, 1964.

[19] D. C. Champeney, *Fourier Transforms and their Physical Applications.* New York: Academic, 1973.

[20] H. P. Schwan and K. R. Foster, "RF field interactions with biological systems: Electrical properties and biophysical mechanism," *Proc. IEEE,* vol. 68, pp. 104–113, 1980.

Konstantina S. Nikita was born in Tripoli, Greece, in 1963. She received the Diploma in electrical engineering and the Ph.D. degree from the National Technical University of Athens, Greece, in 1986 and 1990, respectively. She received the M.D. degree from the University of Athens, Greece, in 1993.

Since 1990, she has been working as a Researcher at the Institute of Communication and Computer Systems, National Technical University of Athens, Greece. Recently, she has been elected Assistant Professor at the Department of Electrical and Computer Engineering, National Technical University of Athens. Her current research interests include applications of electromagnetic waves in medicine, clinical application of hyperthermia, electromagnetic scattering, inverse problems, nonlinear optimization algorithms, and applications.

Nikolaos K. Uzunoglu (M'82) was born in Constantinopole, Turkey, in 1951. He received the B.Sc. degree in electronics from the Technical University of Istanbul in 1973 and the M.Sc. and Ph.D. degrees in 1974 and 1976, respectively, from the University of Essex, England.

He worked from 1977 to 1984, as a Research Scientist at the Office of Research and Technology of the Hellenic Navy. In 1984, he was elected Associate Professor at the National Technical University of Athens, Department of Electrical Engineering, and in 1987 he was promoted to Professor. In 1986, he was elected Vice-Chairman of the Department of Electrical Engineering of the National Technical University of Athens, and in 1988 he was elected Chairman of the same Department. He was reelected as Chairman in 1990 and 1992 twice. In 1991, he was elected and appointed Directer of the Institute of Communication and Computer Systems, an independent research establishment associated with the National Technical University of Athens. His research interests include electromagnetic scattering, propagation of electromagnetic waves, fiber optics telecommunications, and high-speed circuits operating at gigabit/second rates. He has 90 publications in refereed international journals, and he has published three books in Greek on microwaves, fiber optics telecommunications, and radar systems.

In 1981, Dr. Uzunoglu, received the International G. Marconi Award in Telecommunications. Since 1988 he has been the National Representative of Greece to the COST, Technical Telecommunications Committee, actively participating in several COST telecommunications projects. Further, he has been Project Manager of several RACE, ESPRIT, and National Research and Development Projects in the fields of telecommunications and biomedical engineering applications.